Nanofluidic Devices with Two Pores in Series for Resistive-Pulse Sensing of Single Virus Capsids

10 AUTHORS, INCLUDING:

Klaus B Mogensen

Philips

54 PUBLICATIONS   **1,561** CITATIONS

SEE PROFILE

Zhenning Tan

Assembly Biosciences

12 PUBLICATIONS   **128** CITATIONS

SEE PROFILE

Adam Zlotnick

Indiana University Bloomington

124 PUBLICATIONS   **4,340** CITATIONS

SEE PROFILE

Jörg P Kutter

University of Copenhagen

161 PUBLICATIONS   **3,526** CITATIONS

SEE PROFILE

Nanofluidic Devices with Two Pores in Series for Resistive-Pulse Sensing of Single Virus Capsids

Zachary D. Harms[1], **Klaus B. Mogensen**[2], **Pedro S. Nunes**[2], **Kaimeng Zhou**[1], **Brett W. Hildenbrand**[1], **Indranil Mitra**[1], **Zhenning Tan**[3], **Adam Zlotnick**[3], **Jörg P. Kutter**[2], and **Stephen C. Jacobson**[1],*

[1]Department of Chemistry, Indiana University, Bloomington, Indiana 47405

[2]Department of Micro- and Nanotechnology, Technical University of Denmark, Lyngby, Denmark

[3]Department of Molecular and Cellular Biochemistry, Indiana University, Bloomington, Indiana 47405

Abstract

We report fabrication and characterization of nanochannel devices with two nanopores in series for resistive-pulse sensing of hepatitis B virus (HBV) capsids. The nanochannel and two pores are patterned by electron beam lithography between two microchannels and etched by reactive ion etching. The two nanopores are 50-nm wide, 50-nm deep, and 40-nm long and are spaced 2.0-μm apart. The nanochannel that brackets the two pores is 20x wider (1 μm) to reduce the electrical resistance adjacent to the two pores and to ensure the current returns to its baseline value between resistive-pulse events. Average pulse amplitudes differ by <2% between the two pores and demonstrate the fabrication technique is able to produce pores with nearly identical geometries. Because the two nanopores in series sense single particles at two discrete locations, particle properties, e.g., electrophoretic mobility, are determined from the pore-to-pore transit time.

As nanofluidic-based analysis systems become more highly developed, they are finding a more prominent role in the analysis of biomolecules.[1,2] The resistive-pulse technique[3] is a simple and effective tool for label-free, non-destructive detection of single molecules and measures changes in ion current resulting from the transit of particles through an electrically biased nanopore filled with electrolyte. Resistive-pulse sensing of sub-micrometer particles is first reported with track-etched polymer nanopores,[3] and more recent advances in pore fabrication allow analysis of a wide range of samples, e.g., DNA,[4-6] proteins,[7] viruses,[8,9] immune complexes,[10] nanoparticles,[11] and small molecules.[12] Artificial nanopores are made by a number of techniques that include electron beam (e-beam) drilling of SiO_2 membranes[13] and graphene sheets,[14,15] ion-beam milling of pores[16] and channels,[17] soft lithography of nanochannels,[18-20] isolation of carbon nanotubes,[21] and laser pulling of nanopipettes.[22] These artificial nanopores can be fabricated over a large range of lateral dimensions (e.g., 1-1000 nm) and in a variety of geometries (e.g., cylindrical and conical), coupled together in series or in parallel, and integrated into more complex devices.

Viruses are relevant and useful model systems for characterization of nanofluidic devices due to their importance to public health and their biochemical simplicity and uniform physical properties, e.g., charge per unit area and electrophoretic mobility. Like most spherical viruses, the HBV capsid is an icosahedral structure composed of many copies of a single protein. In the case of HBV, the majority of capsids consist of 240 copies of the core

*Corresponding author. jacobson@indiana.edu..

protein arranged with T = 4 icosahedral symmetry.[23] HBV is the subject of extensive biomedical research because of its effects on a global scale: approximately 360 million people suffer from chronic HBV, which leads to approximately 600,000 deaths annually.[24] Furthermore, in the past few years the assembly of HBV and other viruses has arisen as a focus for antiviral research.[25] Simultaneously, viruses have also become a focus of nanotechnology research because of their nanometer size, regular geometry, and conformity on an atomic scale.[26,27] The interest in viruses and their assembly requires further development of techniques that allow interrogation and sorting of individual particles.

Devices with multiple nanopores in parallel are used to increase detection throughput,[28] recognize patterns for multiple analytes,[29] perform multiple immunoassays,[30] increase measurement sensitivity,[31] and conduct fundamental ion transport studies.[32] These examples allow multiple molecules to be measured a single time. However, the ability to probe single molecules multiple times enables the signal-to-noise ratio to be improved and physical properties to be determined. Single DNA molecules are passed back and forth through a single nanopore to make multiple measurements,[33] but these experiments are nontrivial to perform. Two pores are stacked in series in a multilayer device; however, only their electrical properties are reported.[34] The electrophoretic mobility of single molecules can be calculated directly from single-pore resistive pulse measurements[35,36] when the entropic barrier to enter the pore and adsorption to the pore wall are negligible. Electrophoretic mobilities are also determined by measuring fluorescent probes at two locations with two closely spaced laser spots in a capillary.[37] Improvement to these fluorescence measurements is made by confining the samples in submicrometer channels.[38] These experiments, however, are limited to fluorescently labeled molecules.

Our approach is to fabricate a nanochannel with two nanopores in series to sense single particles two times. Our nanochannel devices are patterned in plane by e-beam lithography between two closely spaced microchannels and etched by reactive ion etching. The depth of the nanochannel and pores is controlled by a two-step oxidation process.[39] The two nanopores are 50-nm wide, 50-nm deep, and 40-nm long and are spaced 2.0-μm apart. Integration of the nanochannel with the microchannels permits precise fluid handling and improves mass transfer of the sample to the nanochannel. We chose to characterize our nanofluidic devices with hepatitis B virus (HBV) capsids formed from Cp149, a truncated form of the core protein.[25,40] Average pulse amplitudes for the two nanopores differ by <2%, and electrophoretic mobilities are calculated from the pore-to-pore transit times (i.e., the time needed for the particle to travel from the first pore to the second pore).

Experimental Section

Materials

We purchased 4-(2-hydroxyethyl)-1-piperazineethanesulfonic acid (HEPES) and rhodamine B from Sigma-Aldrich Co.; potassium chloride, potassium hydroxide, sodium chloride, sodium phosphate monobasic, and sodium hydroxide from Mallinckrodt, Inc.; methanol from J.T. Baker Chemical Co.; sodium phosphate dibasic from Amresco, Inc.; B270 substrates and cover plates from Telic Company; silicon substrates from Okmetic Oyj; AZ5214E photoresist from MicroChemicals GmbH; and ZEP520 e-beam resist and ZEP-N50 developer from Zeon Corp.

Device Fabrication

The microchannels and nanochannels with two pores are fabricated in two separate steps. A schematic of the entire device is shown in Figure 1a, and a cross-section of the nanochannel region is shown in Figure 1b. For microchannel fabrication, a 1.5-μm layer of AZ5214E

photoresist is spin-coated onto a blank Si wafer. The microchannel pattern is transferred to the photoresist by UV exposure through a laser-written photomask (Delta Mask BV). After exposure, the photoresist is developed in 1 M NaOH for 50 s and hard-baked at 90 °C for 60 s. The microchannels are then etched into the Si wafer by reactive ion etching (Advanced Silicon Etch, STS) for 12 min. A stylus-based profiler (Dektak 8M, Veeco Instruments, Inc.) is used to measure the microchannel dimensions, which are 10-μm wide and 5.4-μm deep.

For the nanochannel and two pores, e-beam lithography is used to define the width and length, and two thermal oxidation steps to control the depth.[39] An initial oxide layer of 50 nm is thermally grown on the Si wafer with the microchannels. A 120-nm layer of ZEP520 e-beam resist is spin-coated onto the wafer. The nanochannel pattern is transferred to the e-beam resist by e-beam lithography (JBX9300FS, JEOL Ltd.). The e-beam resist is then developed in ZEP-N50, and the nanochannel pattern is etched for 30 s by reactive ion etching (Advanced Oxide Etch, STS) for which the Si wafer acts as the etch stop. The resist is removed in an oxygen plasma at 1000 W for 30 min. The second thermal oxidation step creates a 150 ± 10 nm insulating layer between the nanochannel and Si wafer. The nanochannel is characterized by an atomic force microscope (AFM, Dimension 3000, Veeco Instruments, Inc.) and a scanning electron microscope (SEM, NanoSEM 600, FEI Company). An SEM image of the nanochannel with two pores is shown in Figure 2a. The pores are 50 ± 10 nm wide, 50 ± 5 nm deep, and 40 ± 5 nm long and are spaced 2.0 μm apart. The nanochannel between the two pores is 1.0-μm wide, 50-nm deep, and 1.0-μm long and has a 45° taper to connect to the pores. The nanochannels that connect the pores to the microchannels are 1.0-μm wide and 50-nm deep and have a total length of 37 or 77 μm to span the 40 or 80 μm gap, respectively, between the microchannels.

Prior to bonding the cover plate, holes are sand-blasted into the borosilicate cover plate to give fluidic access to the channels. The borosilicate cover plate is then anodically bonded to the substrate at a potential of 1 kV and temperature of 400 °C for 10 min. Glass reservoirs are epoxied to the open ends of the channels.

Resistive-Pulse Measurements

After fabrication, the channels are sequentially filled with methanol, methanol/water (1:1), water, and 50 mM HEPES buffer with 1 M NaCl at pH 7.5. Current-voltage (IV) curves are recorded with a picoammeter-voltage source (6487, Keithley Instruments, Inc.), and Ag/AgCl electrodes provide electrical contact to the buffer-filled reservoirs. Linear IV behavior confirms that the nanochannels and nanopores do not rectify ion current.

For resistive-pulse sensing, solutions of hepatitis B virus (HBV) capsids (T = 4, 4 MDa, and 36-nm diameter) at 2 or 4×10^7 capsids/mL in 50 mM HEPES buffer with 1 M NaCl are placed in the capsid reservoir. The T = 4 capsid samples are assembled from core protein (Cp149) dimer and purified by sucrose gradient centrifugation.[41] To transport the capsids through the nanochannel that bridges the two microchannels, a positive potential (1.5, 3.0, or 6.5 V) is applied to the waste reservoir, and the capsid reservoir is held at ground (see Figure 1a). An analog output card (PCI-6713, National Instruments Corp.) is used to apply potentials across the device, and the current is amplified (SR570, Stanford Research Systems, Inc.) and recorded at 1 or 10 kHz by a second data acquisition card (PCI-6032E, National Instruments Corp.). Both data acquisition cards are controlled through LabVIEW (National Instruments Corp.). The experiments are conducted inside a Faraday cage.

Resistive-pulse sensing is tested on two devices that have similar dimensions and are denoted device 1 and device 2. For each device, the resistance is calculated by treating the micro- and nanochannels as a series of resistors, for which the resistance in each channel segment is proportional to the channel length divided by the channel cross-section. On

device 1, 68% of the applied potential is dropped across the nanochannel, and 9.3% is dropped between the pores. Results for these experiments are reported as pore-to-pore potentials (V_{pp}) of 0.17, 0.28, and 0.60 V for applied potentials of 1.5, 3.0, and 6.5 V, respectively. Current data are imported into OriginPro 8.5 (OriginLab Corp.) to subtract the baseline current and to determine the pulse amplitude (Δi) and pulse width (w) for each resistive-pulse event and the pore-to-pore transit time (t_{pp}) for each capsid that passes through the two pores in series.

Electroosmotic Flow in Microchannels

The electroosmotic mobility is measured on a glass microfluidic device by making a pinched injection of a zwitterionic dye (e.g., rhodamine B) and measuring its arrival time 1-mm downstream from the injection cross.[42] The glass microfluidic device is fabricated in B270 glass by conventional UV photolithography, wet chemical etching, and cover plate bonding,[43] and is filled with 50 mM HEPES buffer with 1 M NaCl (pH 7.5), which is the same buffer used for the sensing experiments. Electroosmotic transport of rhodamine B (10 μM) at a field strength of 100 V/cm is monitored 1-mm downstream from the cross intersection by laser-induced fluorescence on an inverted microscope (TE2000-U, Nikon, Inc.) equipped with a Ar ion laser at 514.5 nm and photomultiplier tube with a 600-μm spatial filter.[43] The measured electroosmotic mobility is $2.7 \pm 1.5 \times 10^{-6}$ $cm^2V^{-1}s^{-1}$, which correlates well with similar measurements in phosphate buffer with NaCl.

Results and Discussion

The nanofluidic device in Figure 1a has two V-shaped microchannels that are bridged by a single nanochannel with two nanopores in series. The pores are 50-nm wide, 50-nm deep, and 40-nm long and are spaced 2.0 μm apart. The entrance and exit of each pore are designed with 45° tapers to provide a smooth transition to the nanochannel that connects the two pores and for structural support during the fabrication steps of e-beam lithography, reactive ion etching, and cover plate bonding. Thin slit-like pores without any taper tend to collapse or break during these fabrication processes. The width of the nanochannel near each pore is expanded to 1 μm, which is 20x the pore width, to minimize the electrical resistance adjacent to the two pores and to ensure the current returns to its baseline value between sensing events. Figure 2a shows a scanning electron microscope (SEM) image of the nanochannel section with two pores.

We estimate the electric field strength in the nanochannel and pores by dividing the channel into a series of volume elements of uniform length (1 nm) and determining the potential drop across each of those elements. The cross-sectional area of each element (i.e., channel width times depth) varies along the nanochannel, and consequently, the two-dimensional design seen in Figure 2a is incorporated into the calculation. The element length is chosen to be 1-nm long to calculate the resistance in the tapered regions accurately. Figure 2b shows the average electric field strength along the length of the nanochannel-nanopore region for the pore-to-pore potential (V_{pp}) of 0.17 V, and as expected, the highest electric field strengths are localized near the two pores and have maximum values of 8.1×10^3 V/cm. Because the channel width is expanded between the pores, the resistance drops proportionally, which permits the measured current to return to baseline between adjacent resistive-pulse events.

HBV capsids with T = 4 symmetry are 36 nm in diameter, which is comparable to the pore cross-section (50-nm wide by 50-nm deep). Solutions of HBV capsids in 50 mM HEPES buffer with 1 M NaCl are placed in the capsid reservoir. After potentials are applied, the current is monitored over time. Figure 3a shows three two-pulse events that correspond to three capsids electrophoretically migrating through the two-pore device. For the 1.5-V

applied potential, the baseline current for device 1 is 1.9 nA and is subtracted from the current data in Figure 3. Each pair of current pulses has similar amplitude, which indicates that the capsids are not damaged as they translocate through the high electric field regions in the pores. Figure 3b shows an expanded view of the two pulses that correspond to capsid 2 passing through pores 1 and 2. The pulse amplitude (Δi), pore-to-pore transit time (t_{pp}), and pulse width (w) graphically depicted in the figure are discussed in detail below. For data analysis, we make the simplifying assumption that each capsid generates a pair of consecutive pulses, and t_{pp} is obtained from each pair of adjacent pulses.

Histograms of the pulse amplitude (Δi), which is the difference between the baseline current and the pulse minimum, are shown in Figure 4 for pores 1 and 2 for $V_{pp} = 0.17$ V. The histograms indicate that the two pores have comparable dimensions and suggest that the fabrication technique is able to create pores with nearly identical geometries. As seen in Figure 5, Δi differs by <2% between the two pores for all potentials tested and scales with V_{pp}. If we assume the capsids are monodisperse, the relative error in Δi can be attributed to slight differences in the pore dimensions. In addition, $\Delta i/i_{base}$, where i_{base} is the baseline current, is 2-5% at the different applied potentials for both devices, and again, demonstrates that different pores and devices are fabricated and operate similarly.

Additional information is available from the pulse widths of capsids that translocate through the pores. Figure 6 shows pulse width distributions for V_{pp} of 0.17, 0.28, and 0.60 V. Pore-capsid interactions can be modeled by first order kinetics,[44] and these data are fitted with a single exponential function. As V_{pp} increases, the average pulse width (ω) decreases from 8.0 to 2.1 ms. Not only does the transit time decrease as V_{pp} increases, but also the time that the capsids are held up or trapped at the pore decreases, as seen in the nonlinear decrease in average pulse width with V_{pp}.

The pore-to-pore transit time (t_{pp}) is defined as the time needed for a capsid to travel from the first pore to the second pore and is calculated from pairs of adjacent pulses for each capsid (center-to-center). In Figure 7, t_{pp} is plotted for V_{pp} of 0.17, 0.28, and 0.60 V. The primary driving force acting on the HBV capsids is electrophoresis, and therefore, capsid velocity is directly proportional to the charge on the individual capsids and the electric field strength between the two pores. Consequently, an increase in the applied potential corresponds to a decrease in t_{pp} and an increase in capsid velocity (Figure 5). The t_{pp} histograms in Figure 7 are fitted with Gaussian functions, and as expected, the means and standard deviations of the distributions decrease with V_{pp}. These data suggest that two pores in series accurately track particle velocities between resistive-pulse events.

The electrokinetic mobility, μ_{ek}, of the virus capsids can be calculated from the migration time, applied potential, and geometry of the device. We use the migration time from the exit of pore 1 to the entrance of pore 2, i.e., the pore-to-pore transit time (t_{pp}) minus the average pulse width (ω). Because the cross-section of the nanochannel varies between the pores, the electrokinetic mobility is calculated with Equation 1,

$$\mu_{ek} = \frac{1}{(t_{pp} - \omega)} \sum \frac{l_n^2}{V_n}$$

(1)

where l_n is the axial segment length (1 nm) and V_n is the potential difference across that segment. Equation 1 extends the model used to calculate the field strength in Figure 2 and is used to iteratively calculate the average electrokinetic mobility of the virus particles, which is estimated to be $2.1 \pm 1.2 \times 10^{-5}$ cm^{2}V^{-1}s^{-1}.

A high ionic strength buffer (1 M NaCl) is used for the resistive-pulse measurements and significantly reduces the zeta potential at the channel wall, and subsequently, the electroosmotic flow in the nanochannel. However, electroosmotic flow still contributes to the electrokinetic mobility of the virus capsids. Unfortunately, the temporal resolution for electroosmotic mobility measurements made directly on the nanofluidic devices is insufficient for accurate determination. Therefore, the electroosmotic mobility is measured on a glass microfluidic device. For the 50 mM HEPES buffer with 1 M NaCl, the electroosmotic mobility is $2.7 \pm 1.5 \times 10^{-6}$ cm^{2}V^{-1}s^{-1} and is 13% of the electrokinetic mobility of the HBV capsids. For the voltage configuration in Figure 1a, the electroosmotic flow is opposite the direction of the electrophoretic transport of the HBV capsids and must be added to the electrokinetic mobility of the capsids to estimate the electrophoretic mobility of the HBV capsids, $\mu_{ep} = 2.4 \pm 1.2 \times 10^{-5}$ cm^{2}V^{-1}s^{-1}. This value may be slightly underestimated due to the shallow depth of the nanochannel (~50 nm), which can impede capsid transport due to collisions and possible adsorption to the channel walls. To minimize this issue, future device designs will have a similar increase in cross-section, e.g., 20x, but both the channel width and depth will be increased, instead of just the channel width.

Contributions to the standard deviations for the t_{pp} distributions in Figure 7 include diffusion of the capsids, adsorption of the capsids to the channel walls, charge distribution on the surface of the capsids, and geometry of the channel between the two pores, i.e., a particle can travel multiple paths between the two pores. As seen in the SEM image in Figure 2a, the nanochannel is 20x wider than the pores. The shortest geometrical path that a particle can take between the two pores is 2.0 μm, whereas the longest path, which skirts the perimeter of the nanochannel, is 2.4 μm. The average path length that a particle can travel is 2.1 ± 0.1 μm, and the difference in migration paths contributes only 6% to the distribution width. An effective way to narrow these distributions is to modify the surface with a neutral, hydrophilic molecule, e.g., triethylene glycol,[9] which will minimize both particle adsorption and electroosmotic flow.

As seen in Figure 3a, capsid 1 produces a wide pulse at pore 1 and narrow pulse at pore 2, whereas capsids 2 and 3 have similar pulse widths at both pores. For all data sets, the pulse widths at pore 1 exhibit no correlation with the pulse widths at pore 2, when pulse widths for each capsid at pores 1 and 2 are plotted against each other. Moreover, Figure 8 shows no correlation between the time between pulses for any capsid ($t_{pp} - w$) and pulse widths of that capsid at pores 1 and 2. In general, the pulse widths are much wider than expected from the transit time through the pore due to electrophoresis. For example, the transit time of a capsid through a 40-nm pore is 20 μs at an electric field strength of 8.1 kV/cm and electrokinetic mobility of 2.1×10^{-5} cm^{2}V^{-1}s^{-1} However, the average pulse width reported in Figure 6 is 8.0 ms. The data in Figure 8 suggest that the virus particles are held up or trapped due to entropic or dielectrophoretic effects, and the residence times (or pulse widths) at pores 1 and 2 for a capsid are random.

In conclusion, we fabricated nanochannel devices with two pores in series and successfully demonstrated resistive-pulse sensing. The average pulse amplitudes for the two pores differ by <2%, which shows the measurement precision is not limited by the fabrication technique. Consequently, integration of multiple nanopores, e.g., 5 or more pores in series, will enhance the signal-to-noise ratio by the square root of the number of measurements made and improve the counting statistics compared to single nanopore sensors. Furthermore, physical properties of individual virus capsids are easily obtained from the transit time of the capsids from one pore to the next.

Acknowledgments

References

(1). Howorka S, Siwy Z. Chem. Soc. Rev. 2009; 38:2360–2384. [PubMed: 19623355]

(2). Zhou K, Perry JM, Jacobson SC. Annu. Rev. Anal. Chem. 2011; 4:321–341.

(3). DeBlois RW, Bean CP. Rev. Sci. Instrum. 1970; 41:909–916.

(4). Li J, Gershow M, Stein D, Brandin E, Golovchenko JA. Nat. Mater. 2003; 2:611–615. [PubMed: 12942073]

(5). Chen P, Gu JJ, Brandin E, Kim YR, Wang Q, Branton D. Nano Lett. 2004; 4:2293–2298.

(6). Storm AJ, Storm C, Chen JH, Zandbergen H, Joanny JF, Dekker C. Nano Lett. 2005; 5:1193–1197. [PubMed: 16178209]

(7). Sexton LT, Horne LP, Sherrill SA, Bishop GW, Baker LA, Martin CR. J. Am. Chem. Soc. 2007; 129:13144–13152. [PubMed: 17918938]

(8). DeBlois RW, Wesley RKA. J. Virol. 1977; 23:227–233. [PubMed: 196107]

(9). Zhou KM, Li LC, Tan ZN, Zlotnick A, Jacobson SC. J. Am. Chem. Soc. 2011; 133:1618–1621.

(10). Uram JD, Ke K, Hunt AJ, Mayer M. Angew. Chem., Int. Ed. 2006; 45:2281–2285.

(11). Lee S, Zhang YH, White HS, Harrell CC, Martin CR. Anal. Chem. 2004; 76:6108–6115. [PubMed: 15481960]

(12). Heins EA, Siwy ZS, Baker LA, Martin CR. Nano Lett. 2005; 5:1824–1829. [PubMed: 16159231]

(13). Storm AJ, Chen J, Ling X, Zandbergen HW, Dekker C. Nat. Mater. 2003; 2:537–540. [PubMed: 12858166]

(14). Schneider GF, Kowalczyk SW, Calado VE, Pandraud G, Zandbergen HW, Vandersypen LMK, Dekker C. Nano Lett. 2010; 10:3163–3167. [PubMed: 20608744]

(15). Merchant CA, Healy K, Wanunu M, Ray V, Peterman N, Bartel J, Fischbein MD, Venta K, Luo ZT, Johnson ATC, Drndić M. Nano Lett. 2010; 10:2915–2921. [PubMed: 20698604]

(16). Li J, Stein D, McMullan C, Branton D, Aziz MJ, Golovchenko JA. Nature. 2001; 412:166–169. [PubMed: 11449268]

(17). Menard LD, Ramsey JM. Nano Lett. 2011; 11:512–517. [PubMed: 21171628]

(18). Saleh OA, Sohn LL. Nano Lett. 2003; 3:37–38.

(19). Kovarik ML, Jacobson SC. Anal. Chem. 2007; 79:1655–1660. [PubMed: 17297969]

(20). Perry JM, Zhou K, Harms ZD, Jacobson SC. ACS Nano. 2010; 4:3897–3902. [PubMed: 20590127]

(21). Ito T, Sun L, Henriquez RR, Crooks RM. Acc. Chem. Res. 2004; 37:937–945. [PubMed: 15609985]

(22). Wei C, Bard AJ, Feldberg SW. Anal. Chem. 1997; 69:4627–4633.

(23). Seeger, C.; Zoulim, F.; Mason, WS. Fields Virology. Knipe, DM.; Howley, PM., editors. Vol. 2. Lippincott, Williams & Wilkins; Philadelphia: 2007. p. 2977-3029.

(24). WHO Weekly Epidemiological Record. 2004; 79:253–264.

(25). Zlotnick A, Mukhopadhyay S. Trends Microbiol. 2011; 19:14–23. [PubMed: 21163649]

(26). Dragnea B. Nat. Mater. 2008; 7:102–104. [PubMed: 18219330]

(27). Douglas T, Young M. Science. 2006; 312:873–875. [PubMed: 16690856]

(28). McNally B, Singer A, Yu ZL, Sun YJ, Weng ZP, Meller A. Nano Lett. 2010; 10:2237–2244. [PubMed: 20459065]

(29). Zhao QT, Wang D, Jayawardhana DA, Guan XY. Nanotechnology. 2008; 19:505504. [PubMed: 19942772]

(30). Carbonaro A, Sohn LL. Lab Chip. 2005; 5:1155–1160. [PubMed: 16175273]

(31). Ervin EN, White RJ, White HS. Anal. Chem. 2009; 81:533–537. [PubMed: 19140775]

(32). Syeda R, Holden MA, Hwang WL, Bayley HJ. Am. Chem. Soc. 2008; 130:15543–15548.

(33). Gershow M, Golovchenko JA. Nat. Nanotechnol. 2007; 2:775–779. [PubMed: 18654430]

(34). Pedone D, Langecker M, Münzer AM, Wei R, Nagel RD, Rant UJ. Phys.- Condes. Matter. 2010; 22:454115.

(35). Ito T, Sun L, Bevan MA, Crooks RM. Langmuir. 2004; 20:6940–6945. [PubMed: 15274607]

(36). Lan WJ, Holden DA, Zhang B, White HS. Anal. Chem. 2011; 83:3840–3847. [PubMed: 21495727]

(37). Castro A, Shera EB. Anal. Chem. 1995; 67:3181–3186.

(38). Stavis SM, Edel JB, Li YG, Samiee KT, Luo D, Craighead HG. J. Appl. Phys. 2005; 98:044903.

(39). Persson F, Thamdrup LH, Mikkelsen MBL, Jaarlgard SE, Skafte-Pedersen P, Bruus H, Kristensen A. Nanotechnology. 2007; 18:245301.

(40). Katen S, Zlotnick A. Methods in Enzymology. 2009; 455:395–417. [PubMed: 19289214]

(41). Zlotnick A, Palmer I, Kaufman JD, Stahl SJ, Steven AC, Wingfield PT. Acta Crystallogr. Sect. D-Biol. Crystallogr. 1999; D55:717–720. [PubMed: 10089479]

(42). Jacobson SC, Hergenröder R, Koutny LB, Ramsey JM. Anal. Chem. 1994; 66:1114–1118.

(43). Zhuang Z, Starkey JA, Mechref Y, Novotny MV, Jacobson SC. Anal. Chem. 2007; 79:7170–7175. [PubMed: 17685584]

(44). Liebovitch LS, Tóth TI. Bull. Math. Biol. 1991; 53:443–455.
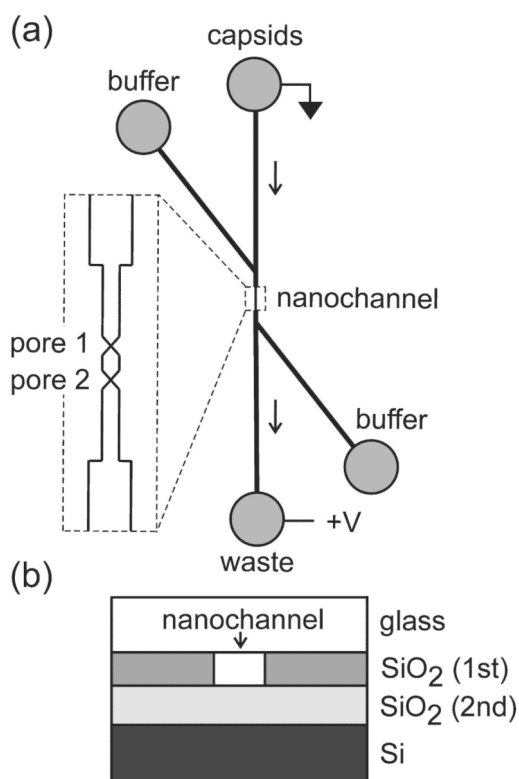
Figure 1.
(a) Schematic of a nanofluidic device with two V-shaped microchannels bridged by a nanochannel with two nanopores in series. Inset is the expanded view of the nanochannel. Arrows depict the direction of the electrophoretic migration of the capsids. (b) Cross-section of nanochannel section of the device layers fabricated by e-beam lithography, reactive ion etching, and two-step thermal oxidation process. Schematics are not to scale.
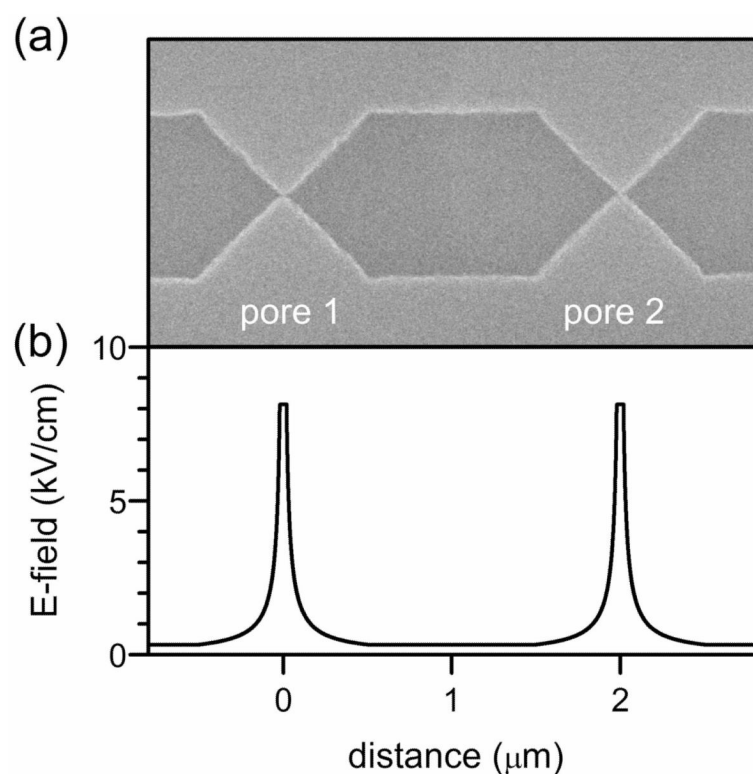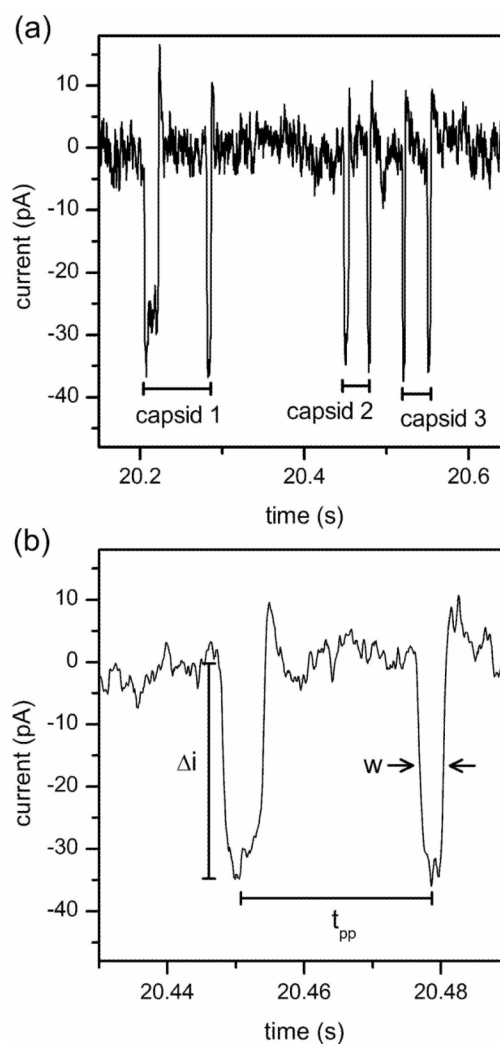
Figure 2.
(a) Scanning electron microscope (SEM) image of a nanochannel with two nanopores in series. Pores 1 and 2 are 50-nm wide, 50-nm deep, and 40-nm long, and the nanochannel between the two pores is 1-μm wide, 50-nm deep, and 1-μm long. The nanochannel tapers at 45° to connect to the two pores, which are spaced 2.0 μm apart. (b) Average electric field strength along the length of the nanochannel for a pore-to-pore potential (V_{pp}) of 0.17 V. The nanochannel in panel (a) is designed to minimize the electrical resistance between the two pores.

Figure 3.
(a) Variation of current with time for T = 4 hepatitis B virus (HBV) capsids that translocate through a nanochannel with two pores in series. Two-pulse events are shown for three HBV capsids. Device 1 and V_{pp} of 0.17 V are used. (b) An enlarged view that shows the two pulses associated with capsid 2. The pulse amplitude (Δi), pore-to-pore transit time (t_{pp}), and pulse width (w) are defined in panel (b), and the 1.9-nA baseline current is subtracted in both panels.
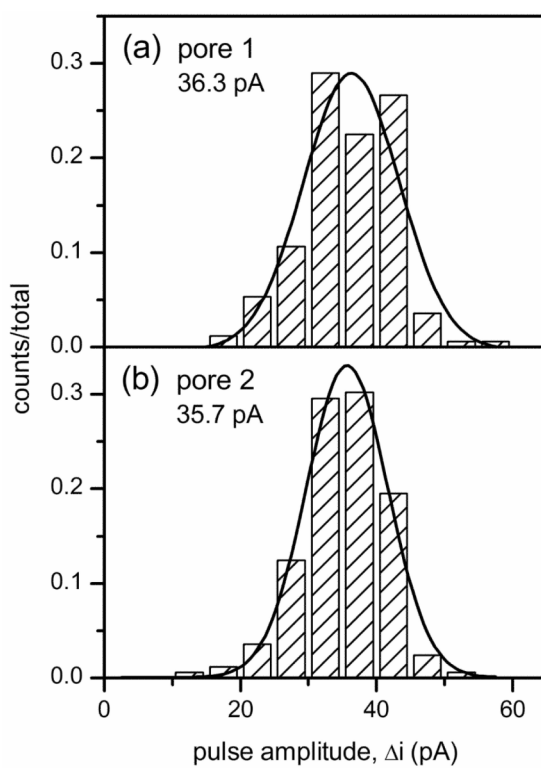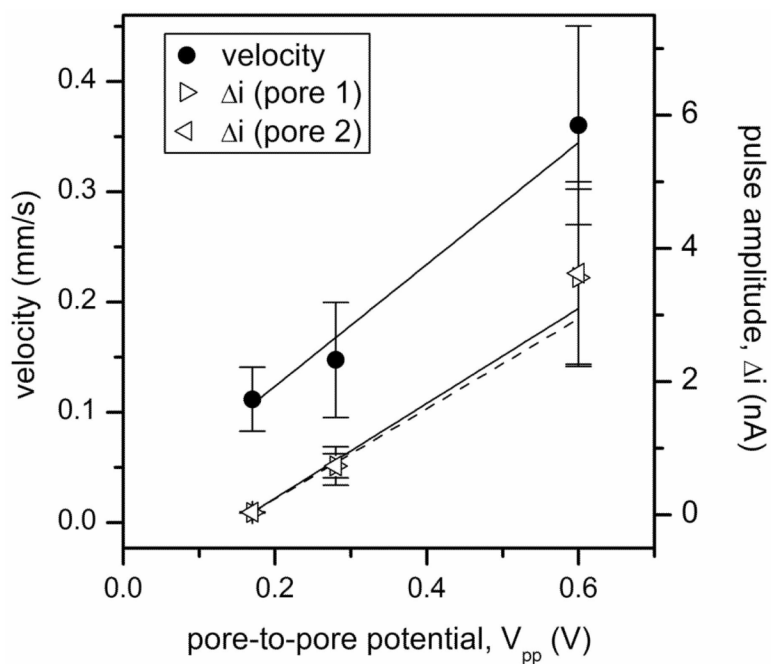
Figure 4.
Histograms of pulse amplitude (Δi) for (a) pore 1 and (b) pore 2 for HBV capsids. Device 1 and V_{pp} of 0.17 V are used. Total counts are 169 for each pore.

Figure 5.
Variation of the velocity and pulse amplitude (Δi) of HBV capsids with pore-to-pore potential (V_{pp}). Pulse amplitudes are calculated from current measurements similar to Figure 3, and velocities are calculated from the pore-to-pore transit times (t_{pp}) in Figure 7.
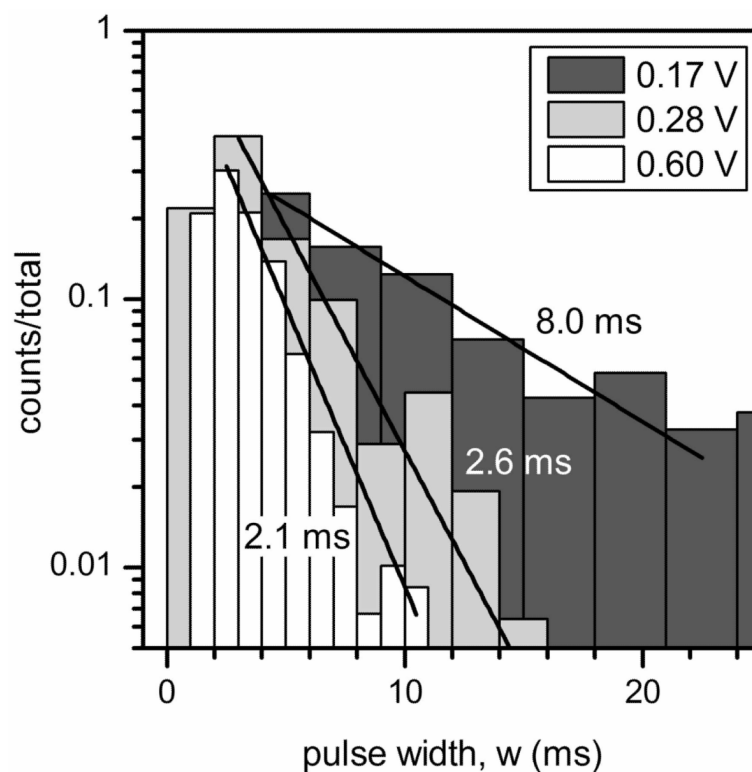
Figure 6.
Histogram of pulse widths (w) for V_{pp} of 0.17, 0.28, and 0.60 V. The data are combined for pores 1 and 2 and are fitted with a single exponential function to obtain average pulse widths (ω) of 8.0, 2.6, and 2.1 ms for V_{pp} of 0.17, 0.28, and 0.60, respectively. Total counts for w are 397 at 0.17 V, 312 at 0.28 V, and 685 at 0.60 V.
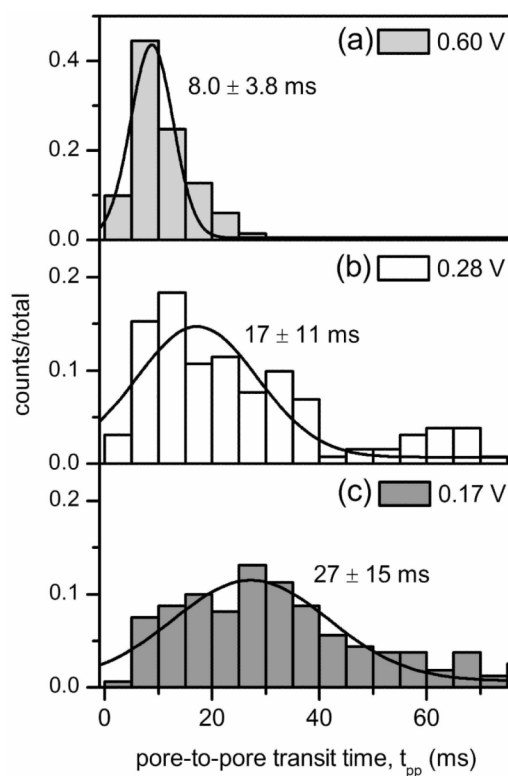
Figure 7.
Histograms of the pore-to-pore transit time (t_{pp}) of HBV capsids for V_{pp} of (a) 0.60 V, (b) 0.28 V, and (c) 0.17 V. The data are fitted with Gaussian functions, and the average times are 8.0, 17, and 27 ms, respectively. Total counts for t_{pp} are (a) 283, (b) 133, and (c) 169.
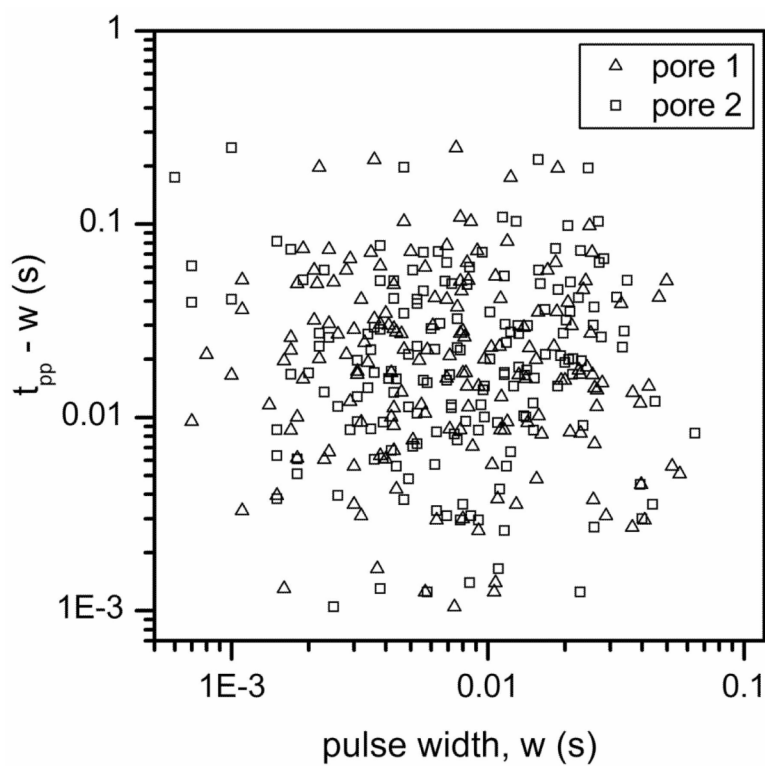
Figure 8.
Variation of the transit time between pulses ($t_{pp} - w$) with pulse width (w) at pores 1 and 2 for each capsid. Device 1 and V_{pp} of 0.17 V are used.